Published in "Nature Materials 8: 310-314, 2009"
which should be cited to refer to this work.

Coexistence of static magnetism and superconductivity in $SmFeAsO_{1-x}F_x$ as revealed by muon spin rotation

A. J. Drew[1,2]*, Ch. Niedermayer[3], P. J. Baker[4], F. L. Pratt[5], S. J. Blundell[4], T. Lancaster[4], R. H. Liu[6], G. Wu[6], X. H. Chen[6], I. Watanabe[7], V. K. Malik[1], A. Dubroka[1], M. Rössle[1], K. W. Kim[1], C. Baines[8] and C. Bernhard[1]*

The recent observation of superconductivity with critical temperatures (T_c) up to 55 K in the pnictide $RFeAsO_{1-x}F_x$, where R is a lanthanide, marks the first discovery of a non-copper-oxide-based layered high-T_c superconductor[1-3]. It has raised the suspicion that these new materials share a similar pairing mechanism to the cuprate superconductors, as both families exhibit superconductivity following charge doping of a magnetic parent material. In this context, it is important to follow the evolution of the microscopic magnetic properties of the pnictides with doping and hence to determine whether magnetic correlations coexist with superconductivity. Here, we present a muon spin rotation study on $SmFeAsO_{1-x}F_x$, with $x = 0$–0.30 that shows that, as in the cuprates, static magnetism persists well into the superconducting regime. This analogy is quite surprising as the parent compounds of the two families have rather different magnetic ground states: itinerant spin density wave for the pnictides contrasted with the Mott–Hubbard insulator in the cuprates. Our findings therefore suggest that the proximity to magnetic order and associated soft magnetic fluctuations, rather than strong electronic correlations in the vicinity of a Mott–Hubbard transition, may be the key ingredients of high-T_c superconductors.

Similar to the cuprates, the pnictide high-critical-temperature (T_c) superconductors (HTSCs) have a layered structure comprising alternating FeAs and LaO sheets, with the Fe arranged on a square lattice[1]. Theoretical calculations predict a quasi-two-dimensional electronic structure, with LaO layers that mainly act as blocking layers and metallic FeAs layers that are responsible for superconductivity[4–6], although these are multiband superconductors with up to five FeAs-related bands crossing the Fermi level[4–7]. Like the copper-oxide HTSCs, the superconducting state in the pnictides emerges on charge doping a magnetic parent compound[8–10], with indications that the maximal T_c occurs just as magnetism disappears[11–13]. The last point may well be of great significance, as the parent compounds in the two families are very different. For the pnictides, there are strong indications that they are itinerant systems with magnetism arising from a nesting-induced spin density wave (SDW). This is in contrast to the cuprates, where it is well established that the mother compounds are 'charge transfer insulators', where strongly repulsive electronic correlations yield an insulating and antiferromagnetic ground state despite a half-filled conduction band. It is therefore of great importance to obtain further insight into the differences and similarities of the pnictide and cuprate HTSCs. A particularly important question is how magnetism and superconductivity evolve on electron doping. In this context, muon spin rotation (μSR) is an ideal technique as it provides microscopic information corresponding to the bulk of a sample and there is a substantial body of μSR data that has been collected on the copper-oxide HTSCs for comparison[14–16].

Here, we present our zero-field μSR (ZF-μSR) measurements, which detail how magnetism evolves with F doping from the SDW state below $T_{mag} \approx 135$ K in the parent compound at $x = 0$ towards the superconducting state at $x \geqslant 0.1$. In particular, we show that static magnetic correlations originating from the FeAs layers survive to a surprisingly high doping level well into the superconducting regime. Figure 1a–e shows representative ZF-μSR spectra, which show the time dependence of the muon spin polarization, $P(t)/P(0)$, at temperatures below and above T_{mag} in the order of increasing F content for $0 \leqslant x \leqslant 0.13$. The solid lines show fits to the experimental data with the function:

$$P(t) = f_1\left(\frac{2}{3}G_{osc} + \frac{1}{3}\right)\exp(-\lambda_1 t)^{\beta_1} + f_2\exp(-\lambda_2 t)^{\beta_2} + f_{bg} \qquad (1)$$

The first term with a fraction f_1 represents the static or quasi-static magnetic signal, the second term with a fraction f_2 the dynamic magnetic signal and the third term a fixed background component due to about 10% of the muons that miss the sample and stop in the sample holder or the cryostat walls. For $x = 0$, the oscillatory part of the magnetic signal takes the form $G_{osc} = \cos(\omega_0 t)\exp(-\sigma^2 t^2)$, whereas $G_{osc} = J_0(\omega_0 t)\exp(-\sigma^2 t^2)$ for $x > 0$. Here, ω_0 is a characteristic precession frequency, σ is a Gaussian relaxation rate reflecting the frequency width and J_0 is a zeroth-order Bessel function. The parameters $\lambda_{1,2}$ and $\beta_{1,2}$ describe the generalized relaxation of the first two components due to magnetic fluctuations. The Bessel function used for $x > 0$ reflects the intrinsic distribution

[1]University of Fribourg, Department of Physics and Fribourg Centre for Nanomaterials, Chemin du Musée 3, CH-1700 Fribourg, Switzerland, [2]Queen Mary University of London, Department of Physics, Mile End Road, London E1 4NS, UK, [3]Laboratory for Neutron Scattering, Paul Scherrer Institut & ETH Zürich, CH-5232 Villigen, Switzerland, [4]Oxford University, Department of Physics, Clarendon Laboratory, Oxford OX1 3PU, UK, [5]ISIS Facility, Rutherford Appleton Laboratory, Chilton, Oxfordshire OX11 0QX, UK, [6]Hefei National Laboratory for Physical Sciences at Microscale and Department of Physics, University of Science and Technology of China, Hefei, Anhui 230026, China, [7]RIKEN-RAL, Nishina Centre, 2-1 Hirosawa, Wako, Saitama, 351-0198, Japan, [8]Laboratory for Muon Spin Spectroscopy, Paul Scherrer Institut, CH-5232 Villigen, Switzerland. *e-mail: A.J.Drew@qmul.ac.uk; christian.bernhard@unifr.ch.

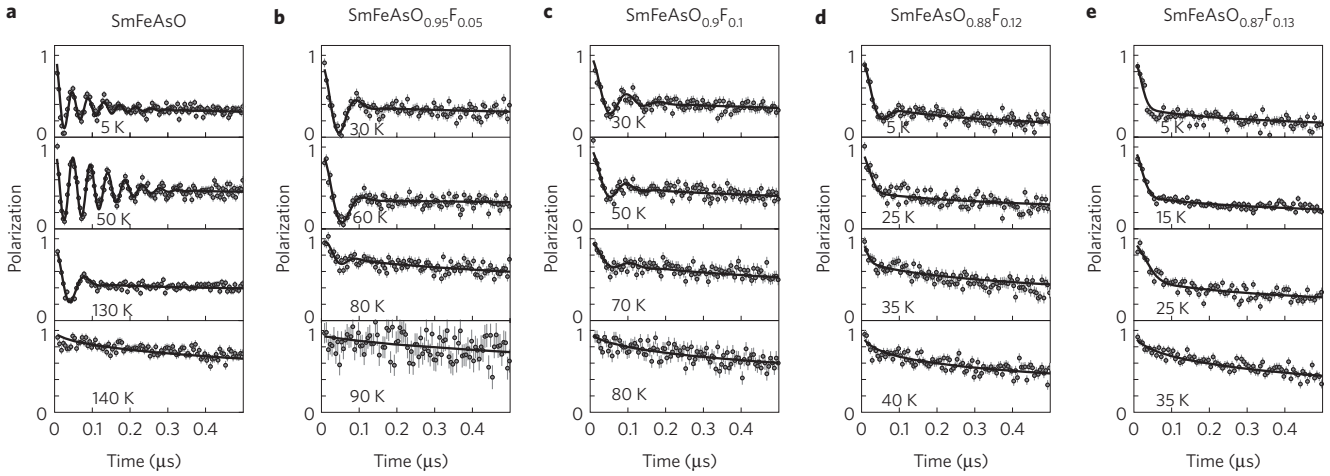

Figure 1 | Temperature and doping dependencies of the ZF-μSR spectra of $SmFeAsO_{1-x}F_x$. a–e, Time-dependent spectra of the muon-spin-polarization, $P(t)/P(0)$, at representative temperatures below and above the magnetic ordering temperature, T_{mag}, for polycrystalline $SmFeAsO_{1-x}F_x$ samples with $x = 0$ and $T_{mag} \approx 135$ K (**a**), $x = 0.05$ and $T_{mag} \approx 80$ K (**b**), $x = 0.1$, $T_{mag} \approx 60$ K and $T_c = 10(7)$ K (**c**), $x = 0.12$, $T_{mag} \approx 35$ K and $T_c = 17(8)$ K (**d**) and $x = 0.13$, $T_{mag} \approx 30$ K and $T_c = 25(8)$ K (**e**). Symbols show experimental data and solid lines fits with equation (1) for which the obtained parameters are shown in Fig. 2a–c.

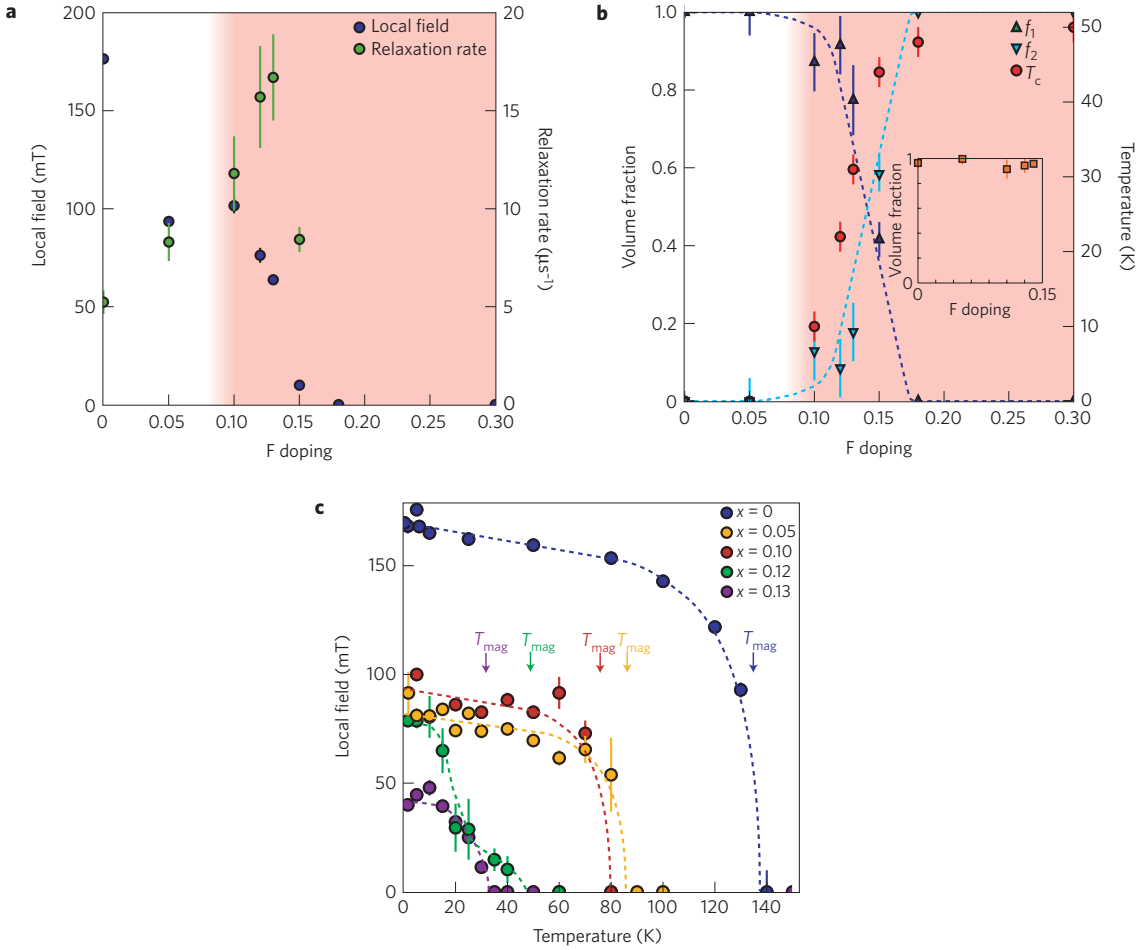

Figure 2 | Evolution of the magnetic signal of the μSR measurements on $SmFeAsO_{1-x}F_x$ as a function of doping and temperature. a, Doping dependence of the local magnetic field, B_μ, and the relaxation rate, λ^{ZF}, as obtained from fitting the ZF-μSR data. The red shaded area marks the superconducting region. **b**, Doping dependence of the amplitudes f_1 and f_2 in the ZF-μSR spectra together with the superconducting transition temperatures, T_c, as obtained from resistivity and magnetization measurements. Inset: Magnetic volume fraction $f_1 + f_2$ obtained from the low-temperature weak transverse-field μSR measurements (using equation (2)). **c**, Temperature dependence of the local field at the muon site, B_μ, as deduced from the precession frequency, ν_μ, in the ZF-μSR spectra with $\nu_\mu = (\gamma_\mu B_\mu / 2\pi)$ and $\gamma_\mu = 2\pi * 135.3$ MHz T^{-1} being the gyromagnetic ratio of the muon. Arrows indicate our estimates of the magnetic transition temperature, T_{mag}.

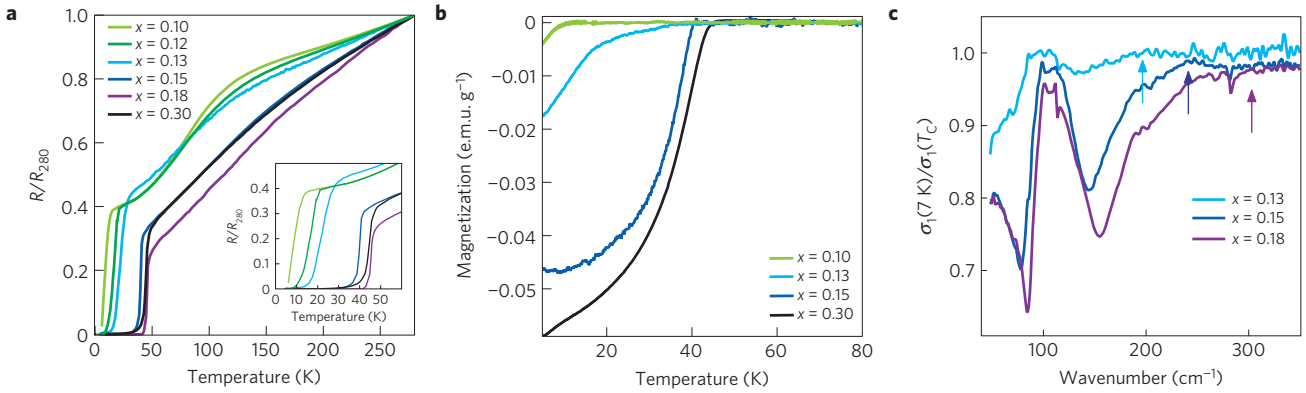

Figure 3 | Evidence for bulk superconductivity due to a gap-like suppression of the infrared optical conductivity, and magnetization and resistivity data supporting the presence of superconductivity. a, Resistivity data, scaled to the resistivity at 280 K, for all of our samples. **b**, Magnetization data, where a sizeable diamagnetic shift is observed for all of the superconducting samples. **c**, Difference spectra of the far-infrared optical conductivity between the normal and the superconducting states for $SmFeAsO_{1-x}F_x$ with $x = 0.13$, 0.15 and 0.18 and $T_c = 25(8)$ K, $T_c = 38(4)$ K and $T_c = 45(3)$ K, respectively. The gap-like suppression is a clear signature of bulk superconductivity. The onset frequency as marked by the arrows is roughly proportional to the superconducting gap energy.

of internal fields associated with an incommensurate SDW (ref. 17). The temperature and doping dependencies of the fitted parameters are summarized in Fig. 2a–c. They establish that bulk and static or quasi-static magnetism persists to a doping level of about $x = 0.13$ and thus survives well into the superconducting regime.

In the first place, this raises the question of whether the magnetism originates from electronic moments within the FeAs layers or is rather due to the ordering of the Sm moments. Our ZF-μSR data establish that all samples for $x \leqslant 0.13$ exhibit fairly high magnetic transition temperatures of $T_{mag} \geqslant 30$ K. This is a clear indication that the magnetic moments originate from the FeAs layers and are not associated with the Sm ions, which order at much lower temperature[18]. The absence of a significant contribution of the Sm moments to the magnetic order at $T \geqslant 10$ K is also confirmed by our ZF-μSR data on the parent material SmFeAsO, of which the precession frequency of 23.6 MHz (see Fig. 2c) is very similar to the frequency observed in LaOFeAs (ref. 10). The static magnetism above 5 K is therefore due to magnetic moments that originate from the FeAs layers. As outlined in Supplementary Information, the ordering of the Sm moments below 5 K is evident in the ZF-μSR data, as well as in our specific heat data for the $x = 0.10$–0.13 samples.

To obtain a quantitative analysis of the magnetic volume fractions, we have carried out further weak transverse-field μSR measurements. In a weak transverse field, the magnetic fraction is not affected by the applied field B and only the non-magnetic terms in equation (1) precess in response to the field, giving the following polarization function:

$$P(t) = f_1\left(\frac{2}{3}G_{osc} + \frac{1}{3}\right)\exp(-\lambda_1 t)^{\beta_1} + f_2\exp(-\lambda_2 t)^{\beta_2} + f_{bg}\cos(\gamma_\mu B t) \quad (2)$$

Any non-magnetic fraction gives rise here to a weakly damped oscillatory signal with an amplitude that can be readily determined. For all samples with $x \leqslant 0.13$, we find that only 10–15% of the muons experience a non-magnetic environment. These are mostly accounted for by the muons that stop outside the sample, either in the sample holder or in the walls and windows of the cryostat. The resulting doping dependence of the magnetic volume fraction is plotted in the inset of Fig. 2b. It highlights that for all samples with $x \leqslant 0.13$, the muons experience static magnetic fields in at least 90% of the sample volume. This does not necessarily imply that the

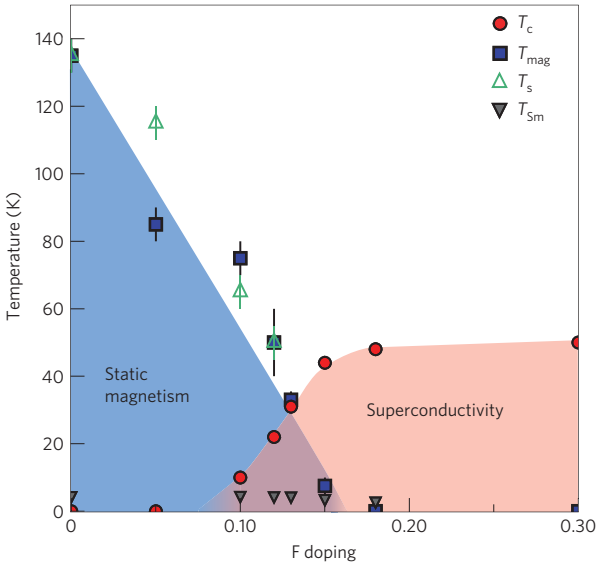

Figure 4 | Phase diagram of the magnetic and superconducting properties of $SmFeAsO_{1-x}F_x$. Evolution of the magnetic transition temperature, T_{mag} (blue squares), the Sm ordering temperature, T_{Sm} (grey triangles[18]), the superconducting transition temperature, T_c (red circles), and the structural transition, T_s (green triangles[24]), as a function of the F substitution and thus electron doping. There is a clear region of coexistence between $x = 0.10$ and 0.15 and T_c reaches its maximal value just as static magnetism disappears.

static magnetic moments exist here in every unit cell. Nevertheless, as the stray fields from antiferromagnetic regions are known to decrease very rapidly, our data suggest that the spatial extent of such non-magnetic regions would be of the order of a few nanometres and thus of the superconducting coherence length as deduced from the upper critical field[19,20] and the gap magnitude[21].

Next we discuss the complementary issue of the superconducting volume fractions. Transverse-field μSR measurements of the vortex state, although they establish a nearly 100% superconducting volume fraction at $x = 0.15$–0.3 (ref. 22), cannot help at $x \leqslant 0.13$, as the relaxation behaviour here is dominated by the magnetism that is already present at T_c. Nevertheless, Fig. 3a,b shows that the resistivity exhibits a fairly sharp drop towards zero and there is a sizeable diamagnetic signal in the magnetization below T_c. In

particular, in Fig. 3c the gap-like suppression of the infrared optical conductivity, σ_1, is a clear signature of bulk superconductivity. This suppression is less pronounced at $x = 0.13$, but this may be understood due to the lower onset frequency and thus gap magnitude[21] (as marked by the arrows) and the reduced condensate density[22,23]. Our infrared data thus are hardly compatible with the point of view that the superconducting volume fraction is more than an order of magnitude smaller at $x = 0.13$ than at $x = 0.15$ and 0.18 where a nearly 100% superconducting volume fraction is established from μSR (ref. 22). Nevertheless, they do not enable us to accurately determine the superconducting volume fraction in these underdoped samples. Accordingly, it remains an open question whether the same or different electronic states contribute to the magnetism and to superconductivity and whether these are spatially homogeneous or phase separated on a microscopic or possibly even on a macroscopic scale, if it is limited to a very small volume fraction.

Irrespective of this open question, our data also provide evidence for a mutual interaction between these two kinds of order. This can be inferred from the doping dependence of the fitting parameters of the ZF-μSR data in Fig. 2a–c, which show that the onset of superconductivity is accompanied by pronounced changes in the magnetic state. For example, the local field, which is a measure of the magnetic order parameter, after a first drop between $x = 0$ and 0.05, remains almost constant between $x = 0.05$ and 0.1, whereas it exhibits a fairly steep decrease at $x > 0.1$ and vanishes near $x = 0.15$. The related sharp maximum in the relaxation rate around $x = 0.12$–0.13 and the decrease of the static magnetic fraction at $x > 0.10$ are furthermore indicative of a fairly sudden loss of magnetic order combined with the onset of slow dynamical fluctuations. We have already previously shown that these slow magnetic fluctuations persist to the highest achievable doping levels[22]. Superconductivity thus seems to appear as soon as the long-range magnetic order is lost and reaches its maximal value in the presence of slow magnetic fluctuations.

Figure 4 summarizes our data in terms of a phase diagram of the superconductivity and magnetism. Also shown are recently reported data of the transition from a tetragonal to orthorhombic structure at low temperature[24], which track the transition temperature of the static magnetism relatively well. This observation agrees with previous reports that the structural transition is a prerequisite for the magnetic one[8]. It shows that the nesting condition of the Fermi surface which stabilizes the SDW state depends rather sensitively on structural details, such as the Fe–As bond angle. Structural differences may also account for the remarkable differences in the phase diagram with respect to $LaFeAsO_{1-x}F_x$ where a recent μSR study found that magnetic correlations are limited to a much narrower doping regime and rather abruptly terminate just before superconductivity occurs at $x \geqslant 0.05$ (ref. 25). A similar magnetic phase diagram has been reported in a recent neutron scattering study on $CeFeAsO_{1-x}F_x$ (ref. 26), where it was argued that static magnetism and superconductivity also do not coexist. Nevertheless, we note that the structural data yield a similar doping dependence of the tetragonal to orthorhombic transition as in the Sm compound[24,26]. Accordingly, we expect that future studies with techniques such as μSR, which are very sensitive to weak and strongly disordered magnetism, may reveal a similar coexistence of strongly disordered magnetism and superconductivity as in $SmFeAsO_{1-x}F_x$.

These substantial differences in the magnetic and superconducting phase diagrams of the La and Sm compounds suggest that the magnetic correlations may have an important role in the HTSC pairing mechanism. Notably, in the Sm compound where static magnetism coexists with superconductivity and slow magnetic fluctuations persist to the highest doping levels[22], the maximal T_c is almost double that of the La compound, where static magnetism disappears abruptly at the onset of superconductivity and spin fluctuations are hardly detectable in the superconducting samples by μSR (refs 25,27,28). Although the static magnetic correlations probably do not contribute to the superconducting pairing interaction, it seems that the slow antiferromagnetic spin fluctuations that emerge in the vicinity of an antiferromagnetic or SDW state may be very beneficial. It is indeed well established that antiferromagnetic spin fluctuations can induce or at least significantly enhance the superconducting pairing, giving rise to HTSCs with an unconventional order parameter[28].

In this context, we also note the similarities with the phase diagram of the cuprate HTSCs, where a comparable coexistence of magnetic correlations and superconductivity has been established[14–16]. Indeed, strongly disordered static magnetism also coexists with superconductivity in the so-called strongly underdoped regime. Furthermore, in the cuprates, the onset of superconductivity gives rise to a suppression of static magnetism and the emergence of slow magnetic fluctuations that persist to higher doping levels, similar to that presented here for $SmFeAsO_{1-x}F_x$. For the cuprate HTSCs, these cannot be followed up to optimal doping with the μSR technique (owing to its limited time window), but they are readily seen, for example, in inelastic neutron scattering[29].

In summary, we have provided evidence that static magnetism in $SmFeAsO_{1-x}F_x$ survives to surprisingly high doping levels. Strongly disordered but static magnetism and superconductivity both exist in the range of $0.1 \leqslant x \leqslant 0.13$ and prominent low-energy spin fluctuations are observed up to the highest achievable doping levels where T_c is maximal. The comparison with similar structural studies suggests that the stability of the SDW state critically depends on the structural details that presumably modify the nesting condition at the Fermi surface or the frustration of competing magnetic interactions. Although many of these structural and electronic details in $SmFeAsO_{1-x}F_x$ are very different from those of the cuprate HTSCs, we find that the magnetic and superconducting phase diagrams as a function of doping are surprisingly similar. Our observations call for a critical examination of the widely accepted point of view that the HTSC pairing mechanism is based on strong electronic correlations in the vicinity of a Mott–Hubbard-type metal to insulator transition. The comparison with the present $SmFeAsO_{1-x}F_x$ superconductors rather points towards an important role of low-energy spin fluctuations that emerge on doping away from an antiferromagnetic or SDW state. A recent work[30] has shown that the actual F content (as measured by energy dispersive X-ray analysis) of the $SmFeAsO_{1-x}F_x$ samples can be lower than the nominal one that is reported in our work. This would lead to a rescaling of the x axis of the phase diagram in our Fig. 4 that would not affect the conclusions presented here.

Methods

Sample preparation and characterization. Polycrystalline samples with nominal composition $SmFeAsO_{1-x}F_x$ with $x = 0.00$, 0.05, 0.10, 0.12, 0.13, 0.15, 0.18 and 0.30 were synthesized by conventional solid-state reaction methods as described in refs 2,11. Standard powder X-ray diffraction patterns were measured where all peaks could be indexed to the tetragonal ZrCuSiAs-type structure. d.c. resistivity and magnetization measurements were made to determine the midpoint (10–90% width) of the resistive and diamagnetic transitions with $T_c = 10(7)$, 17(8), 25(8), 38(4), 45(3) and 45(4) K for $x = 0.1$, 0.12, 0.13, 0.15, 0.18 and 0.3 respectively.

Muon spin rotation. The 100% spin-polarized muon spin rotation/relaxation (μSR) experiments were carried out using the GPS and LTF spectrometers at the Paul Scherrer Institut, Switzerland, for the low-doping samples with $0 \leqslant x \leqslant 0.15$ and using the EMU, ARGUS and MUSR spectrometers at the ISIS Facility, UK, for the samples with $0.15 \leqslant x \leqslant 0.30$. The μSR technique is especially suited for the study of magnetic and superconducting materials as it allows one to study the local magnetic field distribution on a microscopic scale and thus to directly access the volume fractions of the corresponding phases[28,31]. For example, in the case of the strongly underdoped cuprate HTSCs, this technique has been very successfully applied to reveal the coexistence of weak and strongly disordered magnetism and superconductivity[14,15,29,31–33]. Details of this technique are outlined in Supplementary Information.

References

1. Kamihara, Y., Watanabe, T., Hirano, M. & Hosono, H. Iron-based layered superconductor La[$O_{1-x}F_x$]FeAs ($x = 0.05$–0.12) with $T_c = 26$ K. *J. Am. Chem. Soc.* **130**, 3296–3297 (2008).
2. Chen, X. H. *et al.* Superconductivity at 43 K in $SmFeAsO_{1-x}F_x$. *Nature* **453**, 761–762 (2008).
3. Ren, Z. A. *et al.* Superconductivity at 55 K in iron-based F-doped layered quaternary compound Sm[$O_{1-x}F_x$] FeAs. *Chin. Phys. Lett.* **25**, 2215–2216 (2008).
4. Lebegue, S. Electronic structure and properties of the Fermi surface of the superconductor LaOFeP. *Phys. Rev. B* **75**, 035110 (2007).
5. Singh, D. J. & Du, M. H. Density functional study of $LaFeAsO_{1-x}F_x$: A low carrier density superconductor near itinerant magnetism. *Phys. Rev. Lett.* **100**, 237003 (2008).
6. Haule, K., Shim, J. H. & Kotliar, G. Correlated electronic structure of $LaO_{1-x}F_x$FeAs. *Phys. Rev. Lett.* **100**, 226402 (2008).
7. Xu, G. *et al.* Doping-dependent phase diagram of LaOMAs (M = V–Cu) and electron-type superconductivity near ferromagnetic instability. *Europhys. Lett.* **82**, 67002 (2008).
8. de la Cruz, C. *et al.* Magnetic order close to superconductivity in the iron-based layered $LaO_{1-x}F_x$FeAs systems. *Nature* **453**, 899–902 (2008).
9. McGuire, M. A. *et al.* Phase transitions in LaFeAsO: Structural, magnetic, elastic, and transport properties, heat capacity and Mössbauer spectra. *Phys. Rev. B* **78**, 094517 (2008).
10. Klauss, H.-H. *et al.* Commensurate spin density wave in LaFeAsO: A local probe study. *Phys. Rev. Lett.* **101**, 077005 (2008).
11. Liu, R. H. *et al.* Anomalous transport properties and phase diagram of the FeAs-based $SmFeAsO_{1-x}F_x$ superconductors. *Phys. Rev. Lett.* **101**, 087001 (2008).
12. Wen, H., Mu, G., Fang, L., Yang, H. & Zhu, X. Superconductivity at 25 K in hole-doped $(La_{1-x}Sr_x)$OFeAs. *Europhys. Lett.* **82**, 17009 (2008).
13. Luke, G. M. *et al.* Magnetic order and electronic phase diagrams of electron-doped copper oxide materials. *Phys. Rev. B* **42**, 7981–7988 (1990).
14. Niedermayer, Ch. Common phase diagram for antiferromagnetism in $La_{2-x}Sr_xCuO_4$ and $Y_{1-x}Ca_xBa_2Cu_3O_6$ as seen by muon spin rotation. *Phys. Rev. Lett.* **80**, 3843–3846 (1998).
15. Sanna, S., Allodi, G., Concas, G., Hillier, A. D. & De Renzi, R. Nanoscopic coexistence of magnetism and superconductivity in $YBa_2Cu_3O_{6+x}$ detected by muon spin rotation. *Phys. Rev. Lett.* **93**, 207001 (2004).
16. Julien, M. H. Magnetic order and superconductivity in $La_{2-x}Sr_xCuO_4$: A review. *Physica B* **329**, 693–696 (2003).
17. Savici, A. T. *et al.* Muon spin relaxation studies of incommensurate magnetism and superconductivity in stage-4 $La_2CuO_{4.11}$ and $La_{1.88}Sr_{0.12}CuO_4$. *Phys. Rev. B* **66**, 014524 (2002).
18. Ding, L. *et al.* Specific heat of the iron-based high-T_c superconductor $SmO_{1-x}F_x$FeAs. *Phys. Rev. B* **77**, 180510(R) (2008).
19. Zhu, X. *et al.* Upper critical field, Hall effect and magnetoresistance in the iron-based layered superconductor $LaFeAsO_{0.9}F_{0.1-\delta}$. *Supercond. Sci. Tech.* **21**, 105001 (2008).
20. Hunte, F. Two-band superconductivity in $LaFeAsO_{0.89}F_{0.11}$ at very high magnetic fields. *Nature* **453**, 903–905 (2008).
21. Dubroka, A. Superconducting energy gap and c-axis plasma frequency of $(Nd,Sm)FeAsO_{0.82}F_{0.18}$ superconductors from infrared ellipsometry. *Phys. Rev. Lett.* **101**, 097011 (2008).
22. Drew, A. J. *et al.* Coexistence of magnetic fluctuations and superconductivity in the pnictide high temperature superconductor $SmFeAsO_{1-x}F_x$ measured by muon spin rotation. *Phys. Rev. Lett.* **101**, 097010 (2008).
23. Luetkens, H. Field and temperature dependence of the superfluid density in $LaFeAsO_{1-x}F_x$ superconductors: A muon spin relaxation study. *Phys. Rev. Lett.* **101**, 097009 (2008).
24. Margadonna, S. *et al.* Crystal structure and phase transitions across the metal-superconductor boundary in the $SmFeAsO_{1-x}F_x$ ($0 \leq x \leq 0.20$) family. *Phys. Rev. B* **79**, 014503 (2009).
25. Luetkens, H. *et al.* The electronic phase diagram of the $LaO_{1-x}F_x$FeAs superconductor. *Nature Mater.* doi:10.1038/nmat2397 (2009).
26. Zhao, J. *et al.* Structural and magnetic phase diagram of $CeFeAsO_{1-x}F_x$ and its relation to high-temperature superconductivity. *Nature Mater.* **7**, 953–959 (2008).
27. Carlo, J. P. *et al.* MuSR studies of RE(O,F)FeAs (RE = La, Nd, Ce) and LaOFeP systems: Possible incommensurate/stripe magnetism and superfluid density. Preprint at <http://arxiv.org/abs/0805.2186> (2008).
28. Kato, M., Suzumura, Y., Okabe, Y. & Machida, K. Transition temperature enhancement due to aniferromagnetic fluctuations in high-T_c oxide superconductors. *J. Phys. Soc. Jpn* **57**, 726–729 (1988).
29. Fong, H. F. *et al.* Spin susceptibility in underdoped $YBa_2Cu_3O_{6+x}$. *Phys. Rev. B* **61**, 14773–14786 (2000).
30. Hess, C. *et al.* The intrinsic electronic phase diagram of iron-pnictide superconductors. Preprint at <http://arxiv.org/abs/0811.1601> (2008).
31. Schenck, A. *Principles and Applications in Solid State Physics* (Adam Hilger, 1985).
32. Weidinger, A. *et al.* Observation of magnetic ordering in superconducting $La_{2-x}Sr_xCuO_4$ by muon spin rotation. *Phys. Rev. Lett.* **62**, 102–105 (1989).
33. Kiefl, R. F. *et al.* Muon-spin-rotation study of magnetism in $La_{1.85}Sr_{0.15}CuO_4$ and $YBa_2Cu_3O_x$ below 90 mK. *Phys. Rev. Lett.* **63**, 2136–2139 (1989).

Acknowledgements

This work is supported by the Schweizer Nationalfonds (SNF) by grant 200020-119784 and the NCCR program MANEP, the Deutsche Forschungsgemeinschaft (DFG) by grant BE2684/1-3 in FOR538 and the UK EPSRC. We acknowledge helpful discussions with D. Baeriswyl, A. T. Boothroyd and M. Siegrist.

Author contributions

A.J.D, Ch.N., F.L.P., S.J.B., T.L., I.W., C. Baines and C. Bernhard carried out the muon experiments. A.J.D, Ch.N., F.L.P., S.J.B. and C.B(2) analysed and interpreted the results. A.J.D., P.J.B., S.J.B., V.K.M, A.D., M.R., K.W.K. and C.B.(2) were responsible for the characterization measurements. R.H.L., G.W. and X.H.C. prepared the samples.